

# Influence of DNA sequence on the structure of minicircles under torsional stress

Qian Wang<sup>1</sup>, Rossitza N. Irobalieva<sup>2</sup>, Wah Chiu<sup>2,3,4</sup>, Michael F. Schmid<sup>2,3</sup>, Jonathan M. Fogg<sup>3,4,5</sup>, Lynn Zechiedrich<sup>2,3,4,5</sup> and B. Montgomery Pettitt<sup>1,2,\*</sup>

<sup>1</sup>Department of Biochemistry and Molecular Biology, Sealy Center for Structural Biology, University of Texas Medical Branch, Galveston, TX 77555, USA, <sup>2</sup>Graduate Program in Structural and Computational Biology and Molecular Biophysics, Baylor College of Medicine, Houston, TX 77030, USA, <sup>3</sup>Verna and Marrs McLean Department of Biochemistry and Molecular Biology, Baylor College of Medicine, Houston, TX 77030, USA, <sup>4</sup>Department of Molecular Virology and Microbiology, Baylor College of Medicine, Houston, TX 77030, USA and <sup>5</sup>Department of Pharmacology and Chemical Biology, Baylor College of Medicine, Houston TX, 77030, USA

Received January 09, 2017; Revised May 26, 2017; Editorial Decision May 30, 2017; Accepted June 01, 2017

## ABSTRACT

**The sequence dependence of the conformational distribution of DNA under various levels of torsional stress is an important unsolved problem. Combining theory and coarse-grained simulations shows that the DNA sequence and a structural correlation due to topology constraints of a circle are the main factors that dictate the 3D structure of a 336 bp DNA minicircle under torsional stress. We found that DNA minicircle topoisomers can have multiple bend locations under high torsional stress and that the positions of these sharp bends are determined by the sequence, and by a positive mechanical correlation along the sequence. We showed that simulations and theory are able to provide sequence-specific information about individual DNA minicircles observed by cryo-electron tomography (cryo-ET). We provided a sequence-specific cryo-ET tomogram fitting of DNA minicircles, registering the sequence within the geometric features. Our results indicate that the conformational distribution of minicircles under torsional stress can be designed, which has important implications for using minicircle DNA for gene therapy.**

## INTRODUCTION

Although the structure of B-form DNA has been known for over 60 years (1), and the fact that DNA can be supercoiled has been recognized for over 50 years (2), the understanding of DNA supercoiling and the non-B structures that supercoiling facilitates are less complete. DNA supercoiling refers to the overwinding (positive supercoiling) or underwinding (negative supercoiling) of DNA strands. DNA is

maintained in a negatively supercoiled state in most, if not all, organisms. Positive supercoiling and hyper-negative supercoiling are generated transiently during DNA replication (3) and transcription (4,5). Supercoiling has important biological roles in DNA replication (3), DNA transcription (4), gene regulation (6,7), chromosome decatenation (8) and the formation of non-B structures (9). In fact, supercoiling affects almost all aspects of DNA metabolism and allows DNA to be an active participant in its own metabolism (10).

A quantification of supercoiling can be made by counting the linking number,  $Lk$ , which is the number of times one DNA strand wraps around the other. For a given closed-circular DNA double helix,  $Lk$  is a topological invariant (11) that satisfies the following relationship:

$$Lk = Wr + Tw \quad (1)$$

where writhe,  $Wr$ , describes the average number of crossings of the DNA helix with itself seen from all projections and twist,  $Tw$ , describes the coiling of the two strands around the helical axis. The shape of a supercoiled DNA can be modulated by torsional rigidity (affects  $Tw$ ) and bending rigidity (affects  $Wr$ ) and the solution conditions (e.g. electrostatics). Indeed, simulations (12–14), theory (15) and experiments (15,16) agree that torsional stress can lead to supercoiling, base-flipping, kinks, and denaturation, all of which influence the shape of the DNA molecule. These DNA supercoil-mediated structural changes affect how binding proteins, other nucleic acids, and drugs access DNA.

In addition to their value for the study of DNA structure and function, supercoiled DNA minicircles are being utilized for gene therapy (17–24). These DNAs can transfect many clinically relevant cell types that are refractory to transfection with conventional vectors, which are typically several thousand base pairs in length. How DNA shape affects transfection is unknown but we hypothesize that by

\*To whom correspondence should be addressed. Tel: +1 409 772 0723; Email: mpettitt@utmb.edu  
Present address: Rossitza N. Irobalieva, Universität Zürich, 8057 Zurich, Switzerland.

modulating supercoiling and sequence it may be possible to influence the DNA to adopt specific shapes that may further improve transfection. The 3D conformation of DNA is modulated by its supercoiling level and sequence. A better understanding of how supercoiling and sequence modulate DNA shape may allow it to be controlled, which has many possible applications including improved gene therapy vectors.

Many experimental techniques (25–30) have been used to study DNA supercoiling. A recent study combining cryo-electron tomography (cryo-ET), biochemical analyses, and simulations investigated the structural distribution of 336 bp DNA minicircles with specific supercoiling levels (31). That study describes the DNA minicircle structural diversity, modulated by the level of increasing supercoiling, from an open circle, to a ‘figure-8’, a ‘racquet’ (a large loop on one end and the other end highly intertwined with a sharp bend), a ‘needle’ (intertwined with one small loop at one end), to finally a ‘rod’ (all intertwined).

The DNA sequence is not discernable at cryo-ET resolution. Furthermore, whereas all-atom simulations provide high-resolution structures, it is difficult to sample a large variety of initial possible models or simulate beyond tens of nanoseconds. In addition, the majority of published simulation work, even the most recent (32), only includes DNA with minimal torsional stress, and thus cannot interpret how DNA sequence influences conformation.

In this work, we employed coarse-grained simulations and theoretical analyses to model DNA minicircles with the same sequence as previously studied (31) under a wide range of torsional stress, including highly positively and highly negatively supercoiled, not previously simulated. These new simulations provided a way to relate the observed cryo-ET structures with DNA sequence (31). We found that a thermodynamically unstable segment of the minicircle cooperates with a mechanical correlation from the stress of circularization to influence minicircle structure. With this new information, we were able to determine how the sequence, coupled with supercoiling, can modify the structure and provide sequence-specific models for cryo-ET data. We used these findings to computationally design a new three-lobed structure. Overall, our improved coarse-grained modeling qualitatively explains how DNA sequence defines the three-dimensional structures of supercoiled DNA.

## MATERIALS AND METHODS

We used two different simulation procedures. The first sampled the full possible conformational distributions allowed by the model. This unconstrained simulation included the 336 bp minicircle DNA sequence but did not include cryo-ET structural data. The resulting structural distributions were then compared with the distribution of minicircle conformations seen by cryo-ET. The second procedure was a constrained simulation that contained a bias potential to restrain the results to the experimental data.

### Unconstrained simulation

We simulated a 336 bp DNA minicircle of sequence: TTTATACTAACTTGAGCGAAACGGGAAGGGTT

TTCACCGATATCACCGAAACGCGCGAGGCAGC  
TGTATGGCATGAAAGAGTTCTTCCCGGAAAAC  
CGGGTGAATATTTTCGTTTCCTACTACGACTA  
CTATCAGCCGGAAGCCTATGTACTCAGGTTCCG  
ACACTTTCATTGAGAAAGATGCCTCAGCTCTGTT  
ACAGGTCATAATACCATCTAAGTAGTTGATT  
CATAGTGACTGCATATGTTGTGTTTTACAGTATT  
ATGTAGTCTGTTTTTTATGCAAATCTAATTTAA  
TATATTGATATTTATATCATTTTACGTTTCTCGT  
TCAGCTTT. The coarse-grained force field model used was originally developed by the Louis group (33,34). In their model, they used a Morse potential to represent the hydrogen-bonding and stacking interactions between two bases  $i$  and  $j$ :

$$V_{ij} = \varepsilon_{ij}(1 - e^{-(r-r_0)^a})^2 \quad (2)$$

where  $r$  is the distance between two bases,  $r_0$  is the equilibrium distance, and  $a$  is an empirical factor.  $\varepsilon_{ij}$  is determined by two different base pairing (C/G or A/T) and 10 different base stacking combinations (GpC, CpG, ApT, TpA, GpG, GpA, ApG, TpG, GpT, ApA). Therefore, the  $\varepsilon_{ij}$ ’s are sequence dependent. The stability of each base pair largely affects the supercoiling of a DNA minicircle under torsional stress because the least stable base pair serves as one bend location (Figure 4). In addition, the radius of gyration of a supercoiled DNA minicircle can be regulated by modulating the stability of several base pairs (Figure 5). Thus, the choice of a set of  $\varepsilon_{ij}$  is important to this study. The  $\varepsilon_{ij}$  sets were obtained by an analytical fitting procedure to reproduce the melting temperatures of different DNA sequences (33,34). We previously showed that this model successfully predicts the experimental observed structural alterations in plasmid pBR332 under mechanical stress (35), lending credence to the suitability of the model. We note that this model, as well as the main scope of this work, was not to obtain a definitive kinetic time scale for DNA dynamics. Instead, we focus specifically on the conformational distribution of a DNA minicircle in the equilibrated state. As a result, the actual time scales are not calibrated.

Circular DNA conformations change with salt (27,36). Because the original Louis model did not consider the effects of salt, we previously modified it by adding a term approximating the electrostatic interactions between two charged beads in the presence of ions as a Debye–Hückel potential (35):

$$V_{ij} = \frac{\gamma q_i q_j}{4\pi \varepsilon_0 \varepsilon_r r} e^{-r/\sqrt{\varepsilon_0 \varepsilon_r k_B / 2e^2 I}} \quad (3)$$

where  $i$  and  $j$  are the phosphate atoms and  $r$  is the separation between them;  $\varepsilon_0$  is the permittivity of free space,  $\varepsilon_r$  is the relative dielectric constant (set to 80) and  $I$  is the ionic strength of the system.  $\gamma = 0.7$  was an empirical fit obtained in our previous work (35) to match the DNA melting temperatures under the various different salt conditions. We set the ionic strength to 0.1 M and the temperature to 310 K at an effective 1 atm of pressure. Newtonian dynamics were applied and the Andersen thermostat method was used to maintain the temperature (37).

The Watson–Crick strands of a relaxed 336 bp minicircle wrap around each other 32 times, defining  $Lk_0$  (no super-

coiling).  $\Delta Lk$  is the difference between  $Lk$  under a given torsional stress and  $Lk_0$ . We simulated three different positively supercoiled (overwound) topoisomers:  $Lk = 33$  ( $\Delta Lk = +1$ ),  $34$  ( $\Delta Lk = +2$ ) and  $35$  ( $\Delta Lk = +3$ ). We also simulated six negatively supercoiled (underwound) topoisomers  $Lk = 26$  to  $31$  ( $\Delta Lk = -6$  to  $-1$ ) (28). The corresponding superhelical density ranges from  $-0.194$  to  $+0.085$ , which includes the homeostatically maintained level of underwinding measured by several different groups (38–42).

*In silico*, for each linking number,  $Lk$ , we first built a planar circular minicircle without any crossing points ( $Wr = 0$ ). Under this circumstance,  $Lk = Tw$  based on Equation (1). The twisting angle in degrees between each stacking base pair,  $\theta$ , satisfies the following relationship:

$$336 \times \theta = 360 \times Lk \quad (4)$$

We next performed simulations, each initiated from a planar minicircle.  $Lk$  did not change in the simulation but the partition between  $Wr$  and  $Tw$  varied with  $Lk$ , which was directly observed in the simulations.

For each linking number, the system was equilibrated for 15 ns (because this is a coarse-grained model, the time scale is approximate). After the equilibration, each simulation was performed for an additional 60 ns and data were recorded every 150 ps. Each simulation was repeated 240 times with different random starting velocities, making the overall sampling time 14  $\mu$ s for each linking number. The root-mean-square deviation of the minicircle coordinates for the 240 trajectories and an example of a single trajectory are shown in Supplementary Figure S1. These results demonstrate that the minicircle can be equilibrated well within 60 ns of coarse-grained simulation for a single trajectory and the conformational space can be well sampled with 240 trajectories. These data also show that even with a coarse-grained model, many trajectories from different initial conditions were essential to adequately sample the conformational space. The density maps produced were processed in VMD (43).

### Constrained simulations

Simulations were also performed with an introduced bias potential that restrained results to configurations found in the cryo-ET minicircle density data (25). This protocol was developed for all-atom simulations (44) and we previously applied it to a coarse-grained DNA model (45). A bias potential derived from electron microscopy data,  $V_{EM}$ , was added to the original DNA potential model:

$$V_{x_i}^{EM} = \begin{cases} 0 & \text{if } (\varphi < \varphi_c) \\ \varepsilon \times (-\varphi_{x_i}/s) & \text{else} \end{cases} \quad (5)$$

$\varepsilon = 0.05E$  where  $E = 4.14 \times 10^{-20}$  J. The subvolume of the tomogram including the DNA minicircle was mapped onto a grid  $x_i, x_{i+1}, x_{i+2}, \dots$  ( $x$  can be the X, Y, or Z direction). The overall dimension was  $45 \times 100 \times 80$  Å. The bin size  $x_{i+1} - x_i$  was set to 4.52 Å/pixel to match the sampling of the subvolume. In the experiment, the density of each grid point,  $\varphi$ , was measured.  $\varphi$  was scaled with the standard deviation,  $s$ , of  $\varphi$  at all grid points. In the simulation,  $\varphi$  could be read directly from the experimentally obtained cryo-ET density

(31), ranging from  $-0.8$  s to  $0.8$  s in the experiment. Relatively small  $\varphi$ , however, can correspond to the noise that needs to be screened before the simulation. It is difficult to directly infer an accurate cut-off value,  $\varphi_c$ , for the screening process. So, here we set an empirical value,  $\varphi_c = 0.27$  s, because the isosurface of the experimental density map does not change significantly when  $\varphi < 0.27$  s (Supplementary Figure S6). Each bead in the simulation obtains an external force,  $F^{EM}$ , from this biased potential:

$$F_{x_i}^{EM} = \frac{V_{x_i}^{EM} - V_{x_{i+1}}^{EM}}{d} + \frac{V_{x_i}^{EM} - V_{x_{i-1}}^{EM}}{d} \quad (6)$$

where  $d$  is the grid size 4.52 Å and  $x_i$  refers to a grid point. With this constraint, each bead in the simulation will feel the force from  $V^{EM}$ .

The initial structure of the simulation was set to an unbiased planar circle with random orientation relative to the center of the experimental density. The center of mass velocity of the DNA minicircle model was set to zero. Otherwise, the same simulation protocol as described above was performed for the biased refinement simulations. Each biased simulation set consisted of 1200 repeats of 300 ns, giving a total of 360  $\mu$ s. The probability of each base pair in the sequence to bend or kink was determined.

We chose  $\Delta Lk = -2$  (Figure 6) as an example of the DNA minicircle with two bend locations. For the simulation  $\Delta Lk = -2$  we initially adjusted the twisting angle to make sure that  $Lk = 30$  ( $\Delta Lk = Lk - Lk_0 = 30 - 32 = -2$ ) based on Equation (4). This linking number is a topologically invariant during the simulation based on (11). In the previously published experimental work (31), the linking number was modulated by nicking minicircles and enzymatically religating them at various concentrations of ethidium bromide or the archaeal protein, HmfB, to generate underwound or overwound minicircles respectively. The degree of underwinding or overwinding was determined by the ‘band counting’ method using gel electrophoresis. The  $Lk$  designation was further verified by analyzing the products of relaxation by a type II topoisomerase (31).

## RESULTS

### Conformational distribution of DNA minicircles under torsional stress

Cryo-ET revealed an ensemble of 3D structures of DNA minicircles for each of the various  $Lk$ s (31). We tested how well our coarse-grained model predicted the observed conformations and whether we could assign DNA sequence to the cryo-ET structures. We first simulated the distribution of structures for each topoisomer *de novo*. We used the coarse-grained force field model described above at ambient temperature. Thus, we expected to sample a distribution of possible structures corresponding to those found in the flash frozen solution used for the cryo-ET. Indeed, this model could be used to assign DNA sequence within the experimental cryo-ET structures in the cases with sharp kinks or bends.

The conformational distribution of the DNA minicircle is reflected in the free energy map as a function of the writhe (46,47) ( $Wr$ ) and the fraction of contact formations,  $C$  (Fig-

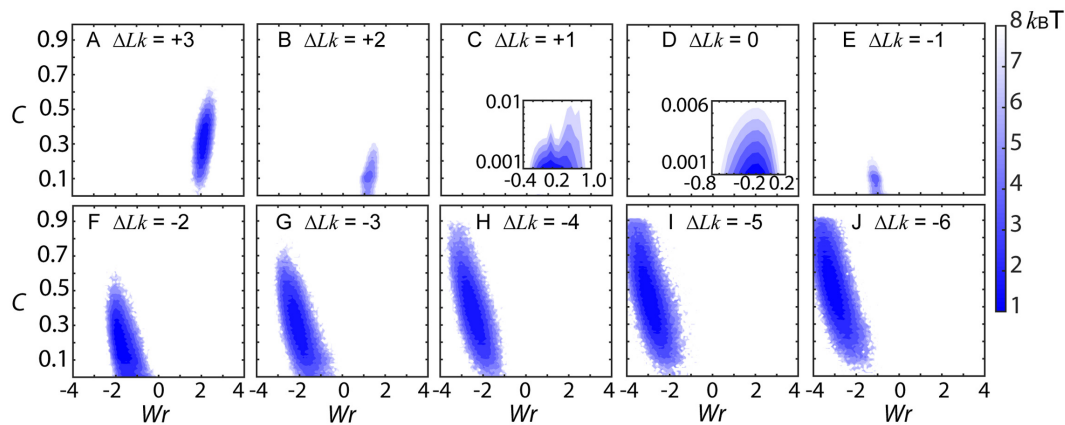


**Figure 1.** Free energy landscape of DNA minicircles under different torsional stress as a function of the percentage of helix-to-helix contacts,  $C$ , and writhe,  $Wr$ . For (C) and (D), insets zoom in to the free energy minimum not seen in the figure scale. The unit of free energy is  $k_B T$  where  $T = 310$  K and  $k_B$  is Boltzmann's constant. Free energy is shown from darkest blue (lowest) to white (highest).

ure 1). A contact formation is defined as an event where the distance between any backbone bead in one base pair and any backbone bead in another base pair is less than  $3\sigma$  ( $\sigma = 8.52$  Å, for details, see Supplementary Information).  $Wr$  measures the average number of crossings of the minicircle seen from all vantage points, while the y-axis,  $C$ , indicates how tightly intertwined the circle is. As a general trend, it is clear that for both positive and negative supercoiling, when the torsional stress increased, both  $Wr$  and  $C$  increased, indicating a higher probability of the DNA becoming more interwound with itself. In addition, the conformational distribution became broader. That is, both  $Wr$  and  $C$  fluctuated more under high torsional stress than low torsional stress. This result is explained by an increase of base pair openings (Table 1) and DNA crossing points that accompanied high torsional stress, which increased the number of possible minicircle conformations. The distribution of the radius of gyration ( $R_g$ ) was also broader under high torsional stress, as shown in Figure 3A.

As expected, the simulated relaxed DNA minicircle ( $\Delta Lk = 0$ ) strongly peaked at  $Wr \sim 0$  and  $C \sim 0$  (Figure 1D). The dominant structure was a nearly planar circle. Roughly 5% of the  $Lk = 32$  circles were warped (Supplementary Figure S2). When  $\Delta Lk = +1$ ,  $C$  and  $Wr$  slightly increased (Figure 1C) and  $\sim 42\%$  became nonplanar (Supplementary Figure S3). With increased positive  $Lk$  ( $\Delta Lk = +2$ ), the probability of nonzero writhe increased. When  $\Delta Lk = +2$ , the dominant (average) structure shifted to the region with  $Wr = 1$  and  $C \sim 10\%$  (Figure 1B), indicating that there is a high probability of a single crossing of the minicircle in the circle. The position of this crossing is identified by the base pair contact map (Figure 2B). Each data point describes the free energy, which was calculated as proportional to the logarithm of the probability of occurrence of a particular contact formation.

We found that the dominant contact formations for  $\Delta Lk = +2$  (blue areas in Figure 2B) were, on average, between bp  $i$  and bp  $j$ , satisfying the relation  $j = x + 168$  (black line in Figure 2A and B), which is half of the total length. Because the total bp of this circle is  $N = 336$ , contact formations are mainly between bp  $i$  and bp  $i + N/2$ . In other words,

the crossing was found close to the center of the circle and evenly split the circle to two roughly equal sub-circles, forming figure-8 shapes. The most common conformation was this figure-8 shape but there were fluctuations from the line  $j = x + 168$ .

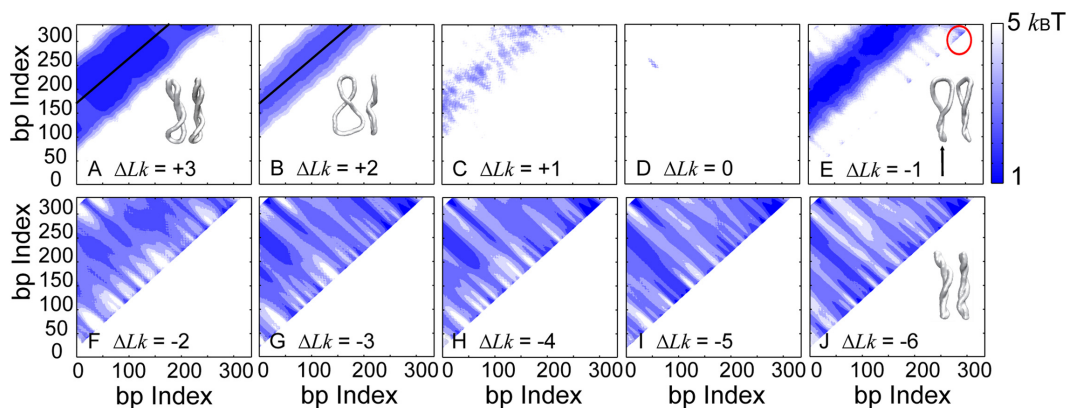
When  $\Delta Lk = +3$ , the average  $Wr$  of the probability distribution of structures centered at 2 (Figure 1A). At the same time, the percentage of close duplex contacts,  $C$ , increased to around 35%, corresponding to a more highly intertwined structure. Considering the base pair contact map for  $\Delta Lk = +3$  (Figure 2A), although the lowest free energy area was still along the line  $j = x + 168$ , the distribution was much broader than it was for the  $\Delta Lk = +2$  minicircle topoisomer (Figure 2B), indicating that a continuous long contact region is formed in the circle between the two crossing points. Such a contact probability formation is reflective of the so-called 'handcuff' configurations in previous experimental observations (31) (Figure 2A).

It is clear that the conformational distribution under negative torsional strain is much broader than that under similar positive strain. This result is not surprising given that negative strain favors base pair opening, which can occur in multiple places to yield different conformations, and moderate positive strain does not. Base-pair opening relieves some of the torsional strain, and makes the structure locally very flexible, more amenable to DNA bending. Table 1 shows the probability of having at least one base pair opening as a function of  $Lk$ . For positive strain, even at the most overwound  $\Delta Lk = +3$  topoisomer studied, there was only a 4.5% probability of base pair opening. In contrast, for negative twist, at  $\Delta Lk = -1$  there was a 10.3% probability of base pair opening, and this probability increased to 100% when  $\Delta Lk < -3$ . These probabilities qualitatively agree with the probability of cleavage by Bal-31 as reported previously (31).

For such a small change in linking number, writhe in the  $\Delta Lk = -1$  topoisomer, centered at  $-1$  and  $C \sim 10\%$  (Figure 1E). The calculation for the  $\Delta Lk = -1$  topoisomer (Figure 2E, black arrow) indicated base pair opening and base unstacking between two consecutive base pairs. As a result, some structures for the  $\Delta Lk = -1$  topoisomer show a so-

**Table 1.** Probability of the DNA minicircle having at least one base pair opening

$\Delta Lk$	0	+1	+2	+3	-1	-2	-3	-4 and above
Probability	0	0	0.6%	4.5%	10.3%	85.0%	99.9%	100%

**Figure 2.** Free energy, in units of  $k_B T$  ( $T = 310$  K), of contact formation between base pairs shown from dark blue (lowest) to white (highest). The black guide line through the blue in (A) and (B) is  $y = x + 168$ . A few representative structures are shown for two views differed by  $90^\circ$ . In (E), the structure represents the typical conformation inside the region circled in red. The arrow shows the position of base pair opening and base unstacking.

called racquet configuration, as seen in the cryo-ET data (31).

With increasing negative torsional stress, negative writhe increased ( $Wr$  decreased) and  $C$  increased (Figure 1F–J). At  $\Delta Lk = -6$ , the most probable  $Wr$  shifted to  $-3.0$  and the maximum of  $C$  was up to 90%, indicating that the most probable minicircle conformation is almost completely wound around itself into a rod shape (Figure 1J). The contact map revealed multiple minima (Figure 2J), indicating that the conformational distribution is very broad.

Overall, the topoisomer structures we obtained *in silico* qualitatively matched the experimental results of Irobalieva *et al.* (31). Both studies agree that with increasing negative supercoiling, DNA minicircles become more intertwined, evolving from an open circle to a figure-8, racquet, needle and finally a rod. We calculated the twist of the minicircle ( $Tw = Lk - Wr$ ) and found that  $Tw$  increased with  $\Delta Lk$  from  $-6$  to  $+3$  (Supplementary Figure S4). These results match well to our previous simulations of twist (with no writhe) at these supercoiling levels (13) and help to further validate the simulation results.

### Effect of torsional stress on minicircle compactness

To understand how the degree and direction of supercoiling compacts minicircles, we considered radius of gyration ( $R_g$ ) (Figure 3).  $R_g$  is a standard measure for polymers and polyelectrolytes and is experimentally accessible via several techniques (48). The radius of gyration of DNA minicircles reduced as a function of torsional stress from  $170$  Å to as small as  $\sim 105$  Å (Figure 3A). Two distinct  $R_g$  maxima, seen for all the negatively supercoiled minicircles and for the most positively supercoiled minicircle, imply two simultaneous populations of structures. We devised a parameter,  $N_v$ , that quantifies the number of bend locations in each minicircle (see Supplemental Information for a complete definition). Figure 3B and C show that the radius of

gyration distribution for three ensembles: all data,  $N_v = 2$ , or  $N_v = 3$ . The existence of the ensemble with  $N_v = 3$  accounts for the mechanism of the size reduction of the DNA minicircle with increasing negative supercoiling.  $N_v = 3$  is a characteristic of compact trefoil structures. Such structures have more bends in order to release the high torsional stress. Several branched structures were seen by cryo-ET (classified as ‘other’) (31).  $N_v = 2$  represents more extended structures like the figure-8 or the handcuff. Generally speaking, the magnitude and distribution of  $N_v$  increased with the increase of torsional stress, and the overall radius of gyration reduced correspondingly.  $R_g$  decreased gradually from  $\Delta Lk = -1$  to  $-3$  (Figure 3A) while at the same range the probability of at least one base pair opening increased from 10% to 100% (Table 1). At this range, although the probability of base pair opening kept increasing,  $N_v$  was only 1 or 2. We suggest that  $R_g$  decreased slowly because the minicircle was more or less in an extended conformation, such as shown in Figure 3B. When  $\Delta Lk$  ranged from  $-4$  to  $-6$ , the probability of  $N_v = 3$  increased, leading to a collapsed structure as shown in Figure 3C (green curve) and causing an even more substantial reduction in the radius of gyration.

### Positive mechanical correlations along DNA minicircles

Because bends affect the conformation of a minicircle, we explored the DNA sequences found at them. We uncovered three thermodynamically unstable segments: bp 1–20, bp 104–115 and bp 287–315, with TpA tracts (TA steps are among the most unstable of the base pair steps (49,50)). We found the same three DNA segments using a separate analytical thermodynamic method (35) (Supplementary Figure S5). If base pair step thermodynamic instability were the only consideration for where sharp bends in the DNA minicircles might occur, one might assume that sharp bends on DNA minicircle would always occur at those thermodynamically unstable segments. We found, however, that this

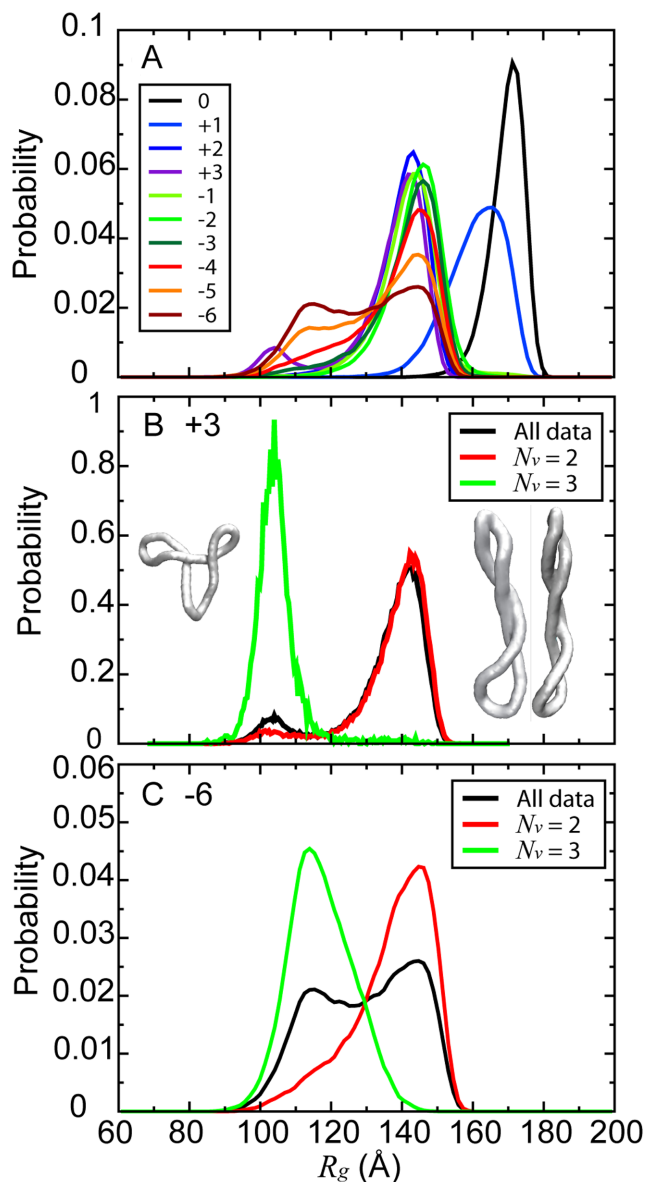


**Figure 3.** Distribution of the radii of gyration for DNA minicircles under torsional stress. (A) Radii of gyration ( $R_g$ ) of DNA minicircles under all the various torsional stresses; (B)  $R_g$  of DNA minicircles at  $\Delta Lk = +3$  for either all data, when  $N_v = 2$  (two sharply bent locations) or when  $N_v = 3$  (three bend locations); (C) same as (B) but for the  $\Delta Lk = -6$  minicircles.

simple notion was not correct. The physical connectivity of the sequences in a circle also influences the bend locations. For example, when  $\Delta Lk = +3$  and  $N_v = 2$ , the bend locations were bp 297 and bp 127 (Figure 4A), which agrees with the experimental mapping using Bal-31 cleavage (31). It is understandable that bp 297 bent because it is among the most thermodynamically unstable (Supplementary Figure S5). The segment surrounding bp 127, however, is more stable than bp 104–115 or bp 1–20. A strong positive mechanical correlation (Figure 4B) exists, then, between bp 297 and 127, which lie roughly at opposite sides of the minicircle. Thus, bp 297 promotes the bending at bp 127. Such corre-

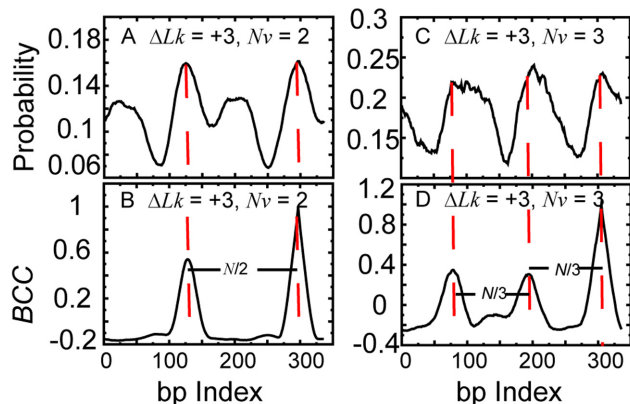


**Figure 4.** Positive mechanical correlations along the DNA minicircle contour length. (A) Probability of becoming the site of a bend location for each base pair for  $\Delta Lk = +3$ ,  $N_v = 2$ ; (B) bend locations correlation coefficient (BCC) between bp 293 and other base pairs, for the  $\Delta Lk = +3$  minicircles,  $N_v = 2$ ; (C) probability of becoming a bend location for each base pair for minicircle  $\Delta Lk = +3$ ,  $N_v = 3$  and (D) bend locations correlation coefficient between bp 305 and other base pairs, for minicircles of  $\Delta Lk = +3$ ,  $N_v = 3$ .  $N$  is the total number of the base pair, 336. Red dashed lines represent the good match between the actual bend location observed in the simulation (A or C) and the position positively correlated to the placement of the first bend (B or D).

lations have been noted previously (32,51) but we make a more general conclusion when  $N_v > 2$  below.

When  $N_v = 3$ , the three bend locations were at bp 305, 195 and 83 (Figure 4C). A positive mechanical correlation among those positions was observed as well (Figure 4D). In addition, the separation among these positions is close to one-third of the total sequence. Our results indicate that instability of the base pair step and the positive mechanical correlation resulting from a thermodynamically weak sequence interacting within the circular DNA constraint together determine the structure/conformational distribution of minicircles under torsional stress.

A general conclusion is that this positive mechanical correlation exists at bp  $(i + N/N_v)\%N$ ,  $(i + 2N/N_v)\%N$ , ...,  $(i + (N_v - 1)N/N_v)\%N$ , where  $N$  is the number of the total base pair,  $N_v$  is the number of the bend locations and % represents the modulo operation (we discuss this further below).

### Modulating supercoiled minicircle conformation by changing DNA sequence

One of the most thermodynamic unstable segments on the supercoiled minicircle is located at bp 303–315, a Tpa tract. Intuitively, changing C/G to A/T at or near a predicted bend location should increase bendability. To test this hypothesis, we designed a new sequence S2. In S2, bp 79–91 was mutated from CTCAAGAAGGCC to ATAAATAATATAA and bp 191–203 was mutated from ACAATGTCCAGTG to ATAATATATATTA. Bp 79–91, 191–203 and 303–315 are three correlated positions when  $N_v = 3$  based on the formula in the previous section. Such mutations should increase the probability of structures with  $N_v = 3$  (relative to  $N_v = 2$ ) and reduce  $R_g$ . Another sequence:  $(AT)_{10}(CG)_{102}(AT)_{10}(CG)_{102}(AT)_{10}(CG)_{102}$  can be considered an extreme case of increasing the probability of

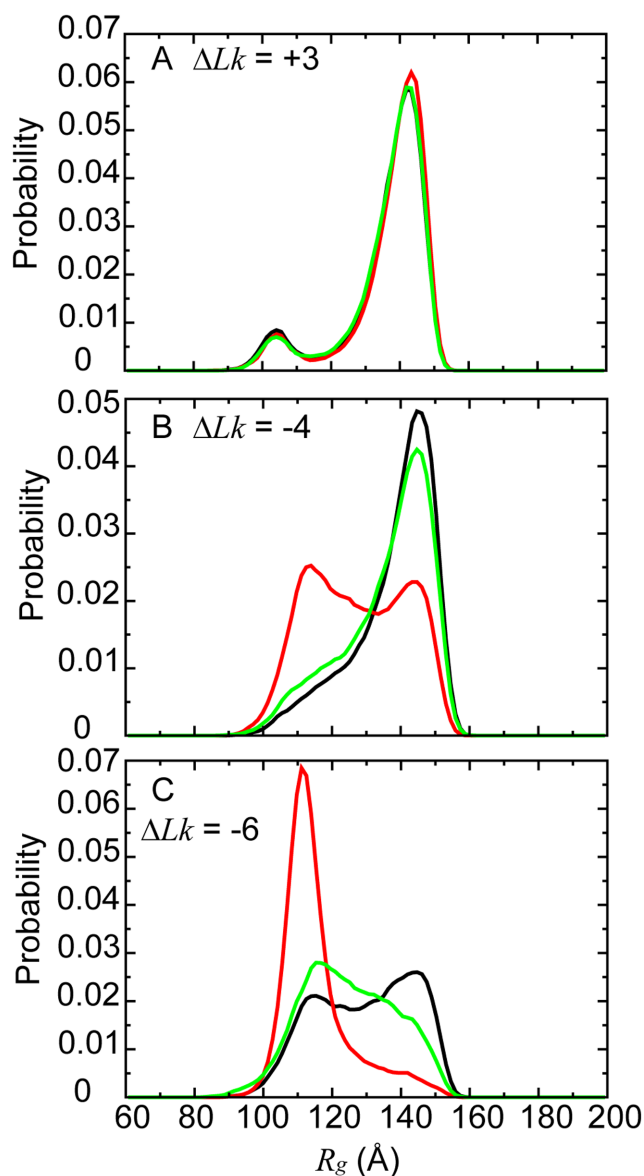


**Figure 5.** Distribution of the radii of gyration for the DNA minicircle and minicircles containing the original sequence (black), sequence S2 (green) or S3 (red) under different torsional conditions: (A)  $\Delta Lk = +3$ , (B)  $\Delta Lk = -4$  and (C)  $\Delta Lk = -6$ .

$N_v = 3$ . Although at  $\Delta Lk = +3$ , the  $R_g$  of all three tested DNA sequences were similar (Figure 5), when  $\Delta Lk = -4$  or  $-6$ , both S2 and S3 shifted to the low  $R_g$  region. This shift indicates that the conformational distribution of minicircles under torsional stress can be designed.

#### Assigning DNA minicircle sequence to cryo-ET conformations

Taking advantage of the bends revealed in the cryo-EM density maps, we probed the probability of each base pair to be involved in a bp opening or unstacking to attempt to locate the sequence with respect to the position of kinked or bent features. Figure 6A shows a cryo-ET density map for  $\Delta Lk = -2$  ( $Lk = 30$ ). This minicircle is in a racquet con-

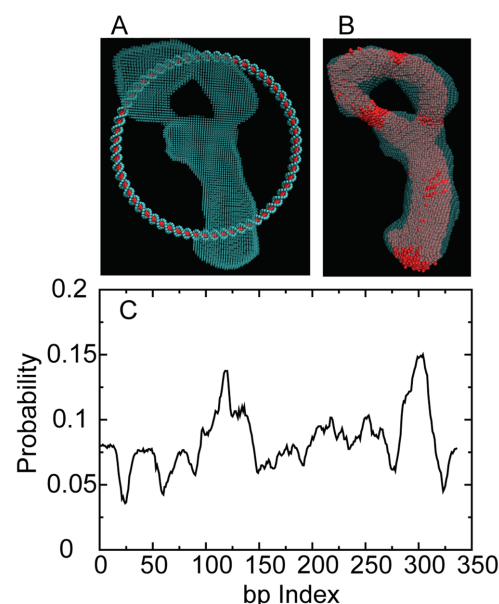


**Figure 6.** Refinement of cryo-ET density map for a structure with  $\Delta Lk = -2$  as an example with two bend locations: (A) an initial structure of a DNA minicircle (the nucleosides are in red and the phosphates are in green) overlaid on the cryo-ET image (cyan, reproduced from the data of Figure 1C in (31)). (B) Superimposition of 250 random structures (red) obtained from the constraint fitting simulation overlaid over cryo-ET image (cyan, produced using the data in Figure 1C in (31)); and (C) the probability of each base pair to become a bend location. This probability is calculated from the occurrence of each base pair forming a bend location observed from 1200 simulations dividing by 1200.

formation and contains a sharp bend at the bottom of the handle of the racquet, as predicted from the analysis above. With a constrained coarse-grained simulation with  $\Delta Lk = -2$  we fitted the molecular structure from the cryo-ET density map at the base pair level. The initial structure of such a simulation can be seen in Figure 6A. A superimposition of 250 simulated structures are shown in Figure 6B. It is clear that with the constraint, our ensemble of structures is in accord with the experimental cryo-ET density map. Whether these simulations of models actually correspond to the actual sequence alignment is difficult to test precisely experimentally but they agree qualitatively with the previously published Bal-31 cleavage results (31). The probability of each base pair to be localized at the bend location as calculated from our extensive set of initial conditions is shown in Figure 6C. Our fitting result indicates that every base pair has some probability of being at the sharp bend but bp 293 and bp 126 have the highest probability. This result qualitatively matches our modelling done without cryo-ET bias constraints (Figure 4A).

#### DISCUSSION

In this work, we studied how the conformational distribution of a 336 bp DNA minicircle changes with torsional stress by performing coarse-grained simulations. These simulations allowed for localized structural deformations by introducing flexible sites that facilitate DNA bending. Therefore, the location of the bends in the conformations of

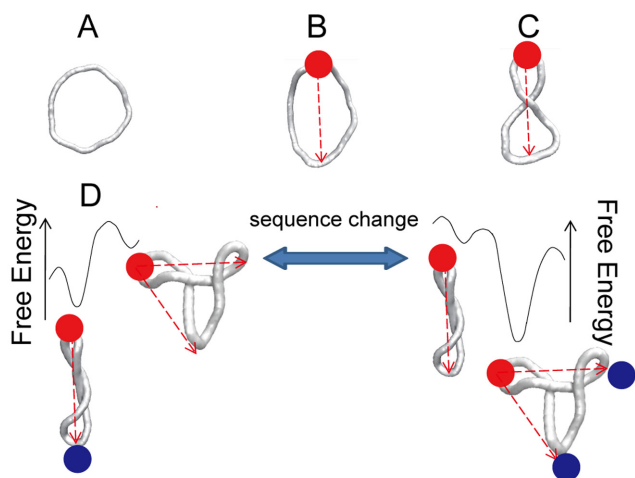


**Figure 7.** Conformational equilibria of a DNA minicircle under negative torsional stress. Negative torsional stress gradually increases from (A) to (D). Red dots mark the most thermodynamic unstable segment along the minicircle. Blue dots mark other thermodynamic unstable segments. Red dash lines represent a strong mechanical correlation. For (D), a dynamic equilibrium exists between two structures: one with two bend locations and one with three. The free energy difference between these two structures depends on the locations of the blue dots that are encoded in the sequence.

supercoiled DNA is modified by sequence. These results demonstrate a useful bridge between the atomic detail provided by all-atom molecular dynamic simulations and the increased conformational sampling that can be achieved by coarse-grained models. Not only did we capture the shape characteristics under each torsional strain condition observed in the experiment, but we were also able to align the DNA sequence in the DNA minicircle in accord with structural and Bal31 nuclease cleavage data (31).

There are several limitations in the accuracy of the current coarse-grained model. The intrinsic curvature (and thus length and supercoiling level) of the minicircle will affect the length and strength of the mechanical correlations detailed above. In order to describe the correlation more quantitatively, the energy functions of different base pairs need to be modelled accurately, which is a difficult task using coarse-grained models. Thus, the results of our current work are qualitative. In addition, proteins, RNA, other DNA, small molecules, etc., can interact with DNA to influence structure (52). Such effects will be studied in the future.

### Mechanical correlations along DNA minicircles

A DNA minicircle under torsional stress may have multiple bends and their locations do not distribute along a minicircle randomly. Instead, we identified a positive mechanical correlation that dictates the separation between two neighbouring bend locations to be  $N_v/N$  ( $N_v$  quantifies the number of bend locations in a minicircle and  $N$  is the total number of base pairs). This correlation was observed thermodynamically (32,53) and kinetically (54) previously. Those studies suggested a  $180^\circ$  cooperative kink along a negatively torsionally stressed DNA minicircle, corresponding to the case of two bend locations ( $N_v = 2$ ) in this work (Figure 7B,C). Our result indicates that  $N_v = 2$  is not the only pos-

sibility for this DNA minicircle under torsional stress. Instead, it has potential to bend with  $N_v = 2$  or  $N_v = 3$  (Figure 4). Importantly, the radius of gyration of a DNA minicircle under torsional stress is largely affected by the number of bend locations ( $N_v$ ).  $N_v = 3$  will lead to significant size reduction, as shown in Figure 3. Thus, the relative probability of  $N_v = 2$  and  $N_v = 3$  will dictate the global structure of a stressed DNA minicircle and this information is encoded by the sequence of the DNA minicircle.

### Assigning sequence registry to DNA cryo-ET density maps

We developed a way that is approximately able to assign DNA sequence registry to the cryo-ET density maps through a geometric penalty function combined with a sequence-sensitive coarse-grained model. The model is computationally sufficiently inexpensive to allow not only shape but sequence registry refinement for low resolution experiments like cryo-ET. The thermodynamically least stable position, as well as its mechanically correlated positions in the minicircle, are more likely to bend and increase the thermodynamic signal of corresponding sequence features and, so, the resulting sequence registry. The bend locations predicted by our constrained simulation (Figure 6C) match well with those predicted by unconstrained simulations (Figure 4A). Further work will require refining the energy function used in the coarse-grained model to determine the bending probability of each base pair more precisely. Once we begin to understand how DNA sequence influences structure/function of DNA, we may begin to understand, for example, how proteins find their sequences, how promoters function, and how DNA metabolism is regulated.

### How sequence affects the conformation of DNA minicircles

In a DNA minicircle stressed by supercoiling, the thermodynamically least stable segment along the sequence has the highest probability of bending. This probability depends on the sequence. AT-rich tracts tend to have the highest probability to bend. Several analytical methods (35,55,56) have been developed to identify the least stable DNA segments under stress more precisely. Once the thermodynamically least stable segment bends, other bend positions will be determined by the mechanical correlations detailed above. The positions of the bends differ depending on the number of them,  $N_v$ . The ensemble of a stressed DNA minicircle can be considered as a mix of bend states, for instance, of  $N_v = 2$  and  $N_v = 3$  (Figure 7D). The probability of  $N_v = 3$ , which corresponds to a small radius of gyration of the minicircle (Figure 3B,C), is influenced by the sequence. If bp  $i + 3/N$  ( $i$  is the thermodynamically least stable position and  $N$  is the total number of base pairs) is thermodynamically unstable (blue dots in Figure 7D on the right), the equilibrium between  $N_v = 2$  and  $N_v = 3$  will shift to the latter and lead to a large reduction in the global size of the minicircle. Indeed, changing the sequence to one that destabilizes the bp  $i + 3/N$  led to a reduction in the radius of gyration (Figure 5B, C). In contrast, if the bp  $i + 2/N$  is thermodynamically unstable (blue dot in Figure 7D on the left), the population of  $N_v = 2$  increased instead and led to an extended structure.

This ability to design conformation should be useful to affect delivery parameters of DNA minicircles in gene therapy delivery.

## SUPPLEMENTARY DATA

Supplementary Data are available at NAR Online.

## ACKNOWLEDGEMENTS

We thank the Louis group for sharing their codes with us. The Sealy Center for Structural Biology scientific computing staff is acknowledged for computational support.

## FUNDING

National Institutes of Health (NIH) [GM 066813 to B.M.P.]; Robert A. Welch Foundation [H-0037 to B.M.P.]; NIH [RO1A1054830, R56AI054830, R01GM115501 to L.Z.]; Human Frontier Science Program (to L.Z.); NIH [P41GM103832 and P50GM103297 to W.C.]; NSF XSEDE via the Texas Advanced Computing Center at The University of Texas at Austin; NSF [CNS-1338192]. Funding for open access charge: NIH; Welch foundation.

*Conflict of interest statement.* J.M.F and L.Z. are co-inventors on issued and pending patents covering the minivector technology in this paper. The funding sponsors had no role in the design of the study; in the collection, analyses, or interpretation of data; in the writing of the manuscript or in the decision to publish the results.

## REFERENCES

- Watson, J.D. and Crick, F.H.C. (1953) Molecular structure of nucleic acids - a structure for deoxyribose nucleic acid. *Nature*, **171**, 737–738.
- Vinograd, J., Lebowitz, J., Radloff, R., Watson, R. and Laipis, P. (1965) Twisted circular form of polyoma viral DNA. *Proc. Natl. Acad. Sci. U.S.A.*, **53**, 1104–1111.
- Stillman, B.W. and Gluzman, Y. (1985) Replication and supercoiling of simian virus-40 DNA in cell-extracts from human-cells. *Mol. Cell. Biol.*, **5**, 2051–2060.
- Liu, L.F. and Wang, J.C. (1987) Supercoiling of the DNA-template during transcription. *Proc. Natl. Acad. Sci. U.S.A.*, **84**, 7024–7027.
- Kouzine, F., Sanford, S., Elisha-Feil, Z. and Levens, D. (2008) The functional response of upstream DNA to dynamic supercoiling *in vivo*. *Nat. Struct. Mol. Biol.*, **15**, 146–154.
- Vonfreisleben, U. and Rasmussen, K.V. (1992) The level of supercoiling affects the regulation of DNA-replication in *Escherichia coli*. *Res. Microbiol.*, **143**, 655–663.
- Ding, Y., Manzo, C., Fulcrand, G., Leng, F.F., Dunlap, D. and Finzi, L. (2014) DNA supercoiling: A regulatory signal for the lambda repressor. *Proc. Natl. Acad. Sci. U.S.A.*, **111**, 15402–15407.
- Witz, G. and Stasiak, A. (2010) DNA supercoiling and its role in DNA decatenation and unknotting. *Nucleic Acids Res.*, **38**, 2119–2133.
- Wang, G. and Vasquez, K.M. (2017) Effects of replication and transcription on DNA structure-related genetic instability. *Genes (Basel)*, **8**, 17.
- Fogg, J.M., Randall, G.L., Pettitt, B.M., Sumners, D.L., Harris, S.A. and Zechiedrich, L. (2012) Bullied no more: when and how DNA shoves proteins around. *Q. Rev. Biophys.*, **45**, 257–299.
- Fuller, F.B. (1978) Decomposition of linking number of a closed ribbon—problem from molecular-biology. *Proc. Natl. Acad. Sci. U.S.A.*, **75**, 3557–3561.
- Mitchell, J.S., Laughton, C.A. and Harris, S.A. (2011) Atomistic simulations reveal bubbles, kinks and wrinkles in supercoiled DNA. *Nucleic Acids Res.*, **39**, 3928–3938.
- Randall, G.L., Zechiedrich, L. and Pettitt, B.M. (2009) In the absence of writhe, DNA relieves torsional stress with localized, sequence-dependent structural failure to preserve B-form. *Nucleic Acids Res.*, **37**, 5568–5577.
- Kannan, S., Kohlhoff, K. and Zacharias, M. (2006) B-DNA under stress: over- and untwisting of DNA during molecular dynamics simulations. *Biophys. J.*, **91**, 2956–2965.
- Jeon, J.H., Adamcik, J., Dietler, G. and Metzler, R. (2010) Supercoiling induces denaturation bubbles in circular DNA. *Phys. Rev. Lett.*, **105**, 4.
- Adamcik, J., Jeon, J.H., Karczewski, K.J., Metzler, R. and Dietler, G. (2012) Quantifying supercoiling-induced denaturation bubbles in DNA. *Soft Matter*, **8**, 8651–8658.
- Kay, M.A. (2011) State-of-the-art gene-based therapies: the road ahead. *Nat. Rev. Genet.*, **12**, 316–328.
- Zhao, N., Fogg, J.M., Zechiedrich, L. and Zu, Y. (2011) Transfection of shRNA-encoding Minivector DNA of a few hundred base pairs to regulate gene expression in lymphoma cells. *Gene Ther.*, **18**, 220–224.
- Catanese, D.J., Fogg, J.M., Schrock, D.E., Gilbert, B.E. and Zechiedrich, L. (2012) Supercoiled Minivector DNA resists shear forces associated with gene therapy delivery. *Gene Ther.*, **19**, 94–100.
- Hardee, C.L., Arévalo-Soliz, L.M., Hornstein, B.D. and Zechiedrich, L. (2017) Advances in non-viral DNA vectors for gene therapy. *Genes (Basel)*, **8**, 65.
- Chen, Z.Y., He, C.Y., Ehrhardt, A. and Kay, M.A. (2003) Minicircle DNA vectors devoid of bacterial DNA result in persistent and high-level transgene expression *in vivo*. *Mol. Ther.*, **8**, 495–500.
- Ribeiro, S., Mairhofer, J., Madeira, C., Diogo, M.M., da Silva, C.L., Monteiro, G., Grabherr, R. and Cabral, J.M. (2012) Plasmid DNA size does affect nonviral gene delivery efficiency in stem cells. *Cell. Reprogramm.*, **14**, 130–137.
- Hornstein, B.D., Roman, D., Arevalo-Soliz, L.M., Engevik, M.A. and Zechiedrich, L. (2016) Effects of circular DNA length on transfection efficiency by electroporation into *HeLa* cells. *PLoS One*, **11**, 17.
- Kreiss, P., Cameron, B., Rangara, R., Mailhe, P., Aguerre-Charriol, O., Airiau, M., Scherman, D., Cruzet, J. and Pitard, B. (1999) Plasmid DNA size does not affect the physicochemical properties of lipoplexes but modulates gene transfer efficiency. *Nucleic Acids Res.*, **27**, 3792–3798.
- Adrian, M., Tenheggelerbordier, B., Wahli, W., Stasiak, A.Z., Stasiak, A. and Dubochet, J. (1990) Direct visualization of supercoiled DNA-molecules in solution. *EMBO J.*, **9**, 4551–4554.
- Boles, T.C., White, J.H. and Cozzarelli, N.R. (1990) Structure of plectonically supercoiled DNA. *J. Mol. Biol.*, **213**, 931–951.
- Bednar, J., Furrer, P., Stasiak, A., Dubochet, J., Egelman, E.H. and Bates, A.D. (1994) The twist, writhe and overall shape of supercoiled DNA change during counterion-induced transition from a loosely to a tightly interwound superhelix - possible implications for DNA-structure *in-vivo*. *J. Mol. Biol.*, **235**, 825–847.
- Levene, S.D., Donahue, C., Boles, T.C. and Cozzarelli, N.R. (1995) Analysis of the structure of dimeric DNA catenanes by electron-microscopy. *Biophys. J.*, **69**, 1036–1045.
- Cherny, D.I. and Jovin, T.M. (2001) Electron and scanning force microscopy studies of alterations in supercoiled DNA tertiary structure. *J. Mol. Biol.*, **313**, 295–307.
- Fogg, J.M., Kolmakova, N., Rees, I., Magonov, S., Hansma, H., Perona, J.J. and Zechiedrich, E.L. (2006) Exploring writhe in supercoiled minicircle DNA. *J. Phys.-Condensed Matter*, **18**, S145–S159.
- Irobalieva, R.N., Fogg, J.M., Catanese, D.J., Sutthitbutpong, T., Chen, M.Y., Barker, A.K., Ludtke, S.J., Harris, S.A., Schmid, M.F., Chiu, W. *et al.* (2015) Structural diversity of supercoiled DNA. *Nat. Commun.*, **6**, 10.
- Sutthitbutpong, T., Matek, C., Benham, C., Slade, G.S., Noy, A., Laughton, C., Doye, J.P.K., Louis, A.A. and Harris, S.A. (2016) Long-range correlations in the mechanics of small DNA circles under topological stress revealed by multi-scale simulation. *Nucleic Acids Res.*, **44**, 9121–9130.
- Ouldrige, T.E., Louis, A.A. and Doye, J.P.K. (2011) Structural, mechanical, and thermodynamic properties of a coarse-grained DNA model. *J. Chem. Phys.*, **134**, 22.
- Sulc, P., Romano, F., Ouldrige, T.E., Rovigatti, L., Doye, J.P.K. and Louis, A.A. (2012) Sequence-dependent thermodynamics of a coarse-grained DNA model. *J. Chem. Phys.*, **137**, 14.

35. Wang, Q. and Pettitt, B.M. (2014) Modeling DNA thermodynamics under torsional stress. *Biophys. J.*, **106**, 1182–1193.
36. Mitchell, J.S. and Harris, S.A. (2013) Thermodynamics of writhe in DNA minicircles from molecular dynamics simulations. *Phys. Rev. Lett.*, **110**, 5.
37. Andersen, H.C. (1980) Molecular-dynamics simulations at constant pressure and-or temperature. *J. Chem. Phys.*, **72**, 2384–2393.
38. McClellan, J.A., Boublikova, P., Palecek, E. and Lilley, D.M.J. (1990) Superhelical torsion in cellular DNA responds directly to environmental and genetic-factors. *Proc. Natl. Acad. Sci. U.S.A.*, **87**, 8373–8377.
39. Sinden, R.R., Carlson, J.O. and Pettijohn, D.E. (1980) Torsional tension in the DNA double helix measured with trimethylpsoralen in living *Escherichia coli* cells - analogous measurements in insect and human-cells. *Cell*, **21**, 773–783.
40. Peter, B.J., Arsuaga, J., Breier, A.M., Khodursky, A.B., Brown, P.O. and Cozzarelli, N.R. (2004) Genomic transcriptional response to loss of chromosomal supercoiling in *Escherichia coli*. *Genome Biol.*, **5**, 16.
41. Zechiedrich, E.L., Khodursky, A.B. and Cozzarelli, N.R. (1997) Topoisomerase IV, not gyrase, decatenates products of site-specific recombination in *Escherichia coli*. *Genes Dev.*, **11**, 2580–2592.
42. Zechiedrich, E.L., Khodursky, A.B., Bachellier, S., Schneider, R., Chem, D.R., Lilley, D.M.J. and Cozzarelli, N.R. (2000) Roles of topoisomerases in maintaining steady-state DNA supercoiling in *Escherichia coli*. *J. Biol. Chem.*, **275**, 8103–8113.
43. Humphrey, W., Dalke, A. and Schulten, K. (1996) VMD: Visual molecular dynamics. *J. Mol. Graph. Model.*, **14**, 33–38.
44. Trabuco, L.G., Villa, E., Mitra, K., Frank, J. and Schulten, K. (2008) Flexible fitting of atomic structures into electron microscopy maps using molecular dynamics. *Structure*, **16**, 673–683.
45. Wang, Q., Myers, C.G. and Pettitt, B.M. (2015) Twist-induced defects of the p-ssp7 genome revealed by modeling the cryo-EM density. *J. Phys. Chem. B*, **119**, 4937–4943.
46. Klenin, K. and Langowski, J. (2000) Computation of writhe in modeling of supercoiled DNA. *Biopolymers*, **54**, 307–317.
47. Levitt, M. (1983) Protein folding by restrained energy minimization and molecular-dynamics. *J. Mol. Biol.*, **170**, 723–764.
48. Flory, P.J. (1989) *Statistical Mechanics of Chain Molecules*. Hanser Gardner Publications, Cincinnati.
49. SantaLucia, J. (1998) A unified view of polymer, dumbbell, and oligonucleotide DNA nearest-neighbor thermodynamics. *Proc. Natl. Acad. Sci. U.S.A.*, **95**, 1460–1465.
50. Olson, W.K., Gorin, A.A., Lu, X.J., Hock, L.M. and Zhurkin, V.B. (1998) DNA sequence-dependent deformability deduced from protein-DNA crystal complexes. *Proc. Natl. Acad. Sci. U.S.A.*, **95**, 11163–11168.
51. Demurtas, D., Amzallag, A., Rawdon, E.J., Maddocks, J.H., Dubochet, J. and Stasiak, A. (2009) Bending modes of DNA directly addressed by cryo-electron microscopy of DNA minicircles. *Nucleic Acids Res.*, **37**, 2882–2893.
52. Wei, J., Czaplak, L., Grosner, M.A., Swigon, D. and Olson, W.K. (2014) DNA topology confers sequence specificity to nonspecific architectural proteins. *Proc. Natl. Acad. Sci. U.S.A.*, **111**, 16742–16747.
53. Lionberger, T.A., Demurtas, D., Witz, G., Dorier, J., Lillian, T., Meyhofer, E. and Stasiak, A. (2011) Cooperative kinking at distant sites in mechanically stressed DNA. *Nucleic Acids Res.*, **39**, 9820–9832.
54. Wang, Q. and Pettitt, B.M. (2016) Sequence affects the cyclization of DNA minicircles. *J. Phys. Chem. Lett.*, **7**, 1042–1046.
55. Peyrard, M. and Bishop, A.R. (1989) Statistical-mechanics of a nonlinear model for DNA denaturation. *Phys. Rev. Lett.*, **62**, 2755–2758.
56. Fye, R.M. and Benham, C.J. (1999) Exact method for numerically analyzing a model of local denaturation in superhelically stressed DNA. *Phys. Rev. E*, **59**, 3408–3426.